

Graph Signal Processing for Global Stock Market Realized Volatility Forecasting

Zhengyang Chi, Junbin Gao, and Chao Wang*

Discipline of Business Analytics, The University of Sydney Business School

Abstract

This paper introduces an innovative realized volatility (RV) forecasting framework that extends the conventional Heterogeneous Auto-Regressive (HAR) model via integrating the Graph Signal Processing (GSP) technique. The volatility spillover effect is embedded and modeled in the proposed framework, which employs the graph Fourier transformation method to effectively analyze the global stock market dynamics in the spectral domain. In addition, convolution filters with learnable weights are applied to capture the historical mid-term and long-term volatility patterns. The empirical study is conducted with RV data of 24 global stock market indices with around 3500 common trading days from May 2002 to June 2022. The proposed model's short-term, middle-term and long-term RV forecasting performance is compared with various HAR type models and the graph neural network based HAR model. The results show that the proposed model consistently outperforms all other models considered in the study, demonstrating the effectiveness of integrating the GSP technique into the HAR model for RV forecasting.

Keywords: volatility spillover; realized volatility; graph signal processing; spectral analysis.

*Corresponding author. Email for all authors: {zhengyang.chi, junbin.gao, chao.wang}@sydney.edu.au

1 Introduction

In the complex ecosystem of global financial markets, understanding and forecasting volatility is important for investors, risk managers and policymakers. Recent studies on financial volatility analysis have emphasized the volatility spillover phenomenon, which refers to the transmission of volatility shocks from one market to others globally (Kanas, 2000; Forbes and Rigobon, 2002; Poon and Granger, 2003; Diebold and Yilmaz, 2009; Yang and Zhou, 2017; Bollerslev et al., 2018). This phenomenon has gained much attention, especially after the highly volatile 2008 global financial crisis (GFC) and the recent COVID-19. The significance of the volatility spillover effect necessitates a comprehensive volatility forecasting framework to consider both the cross-sectional volatility inter-relationship among different financial assets and the temporal autocorrelation of the volatility of each asset.

Various financial volatility measurements have been suggested in the literature (Poon and Granger, 2003). Among different measurement approaches, the high frequency data based Realized Variance (RV), proposed by Andersen and Bollerslev (1998), is particularly useful for capturing the intraday fluctuations in financial time series and is extensively used in the financial practice. The daily RV is calculated as the sum of squared intraday high frequency returns. The Heterogeneous Auto-Regressive (HAR) model, initially introduced by Corsi (2009) and later extended by numerous studies, such as Patton and Sheppard (2015); Bollerslev et al. (2018), stands out as a frequently employed model in RV forecasting due to its effectiveness and simplicity. The conventional HAR type models cannot capture the volatility spillover effect among different assets. To address this, several HAR model extensions, including the Vector HAR (VHAR) model (Bubák et al., 2011), the HAR Kitchen Sink (HAR-KS) model (Liang et al., 2020) and the Graph Neural Network HAR model (GNNHAR) model (Zhang et al., 2025) are proposed. Meanwhile, all these extensions incorporate the volatility spillover effects into the HAR framework by treating them as exogenous variables, via simultaneously considering the spatial and temporal relationships of volatility dynamics.

With the development of graph signal processing (GSP) technique, which extends the traditional signal processing methods to graphical data, the volatility spillover effect and the volatility auto-regressive process can be analyzed not only in the spatial and temporal domains, but also in the graph spectral domain. Comparing to the existing volatility forecasting studies which are limited to spatial and temporal domain, incorporating the additional graph spectral domain to model the volatility spillover effect can help fully explore the inherent structure of the volatility dynamics and identify both the local and global pattern of the multi-asset volatility interrelationships. However, the current literature lacks explorations

of GSP-related strategies to effectively integrate the volatility spillover effect within the HAR framework. Motivated by the identified gap, this research proposes a novel framework based on the GSP technique to embed the volatility spillover effect in the HAR model. The proposed framework is referred to as the GSPHAR. The main contributions of this research are summarized below:

- The proposed GSPHAR framework is the first attempt to explore a GSP-based strategy to incorporate the volatility spillover effect into the HAR model. The GSPHAR framework does not treat the volatility interrelationships as exogenous variables in the HAR model. Rather, the volatility spillover effect is prioritized and embedded in the design of the proposed framework. Empirical results show that the proposed approach can embed and effectively capture the volatility spillover effects in the HAR framework and significantly enhance the RV forecasting accuracy.
- Via employing the convolution filters with learnable weights, the proposed GSPHAR framework incorporates more flexible volatility auto-regressive process, comparing to the existing HAR type models. The decaying pattern of the influence from historical volatility to future volatility does not only exist between the short-term, mid-term and long-term periods as the HAR does, but it also occurs at higher granularity within the mid-term and long-term periods.
- The proposed GSPHAR framework allows extra designs to integrate the changing volatility interrelationships into RV forecasting tasks. These designs allow the proposed framework to capture the dynamic nature of the volatility spillover effect, which is overlooked in the other HAR model extensions mentioned above.

The paper is organized as follows. Section 2 provides preliminaries of pertinent concepts and models. The proposed framework is developed in Section 3. Section 4 presents the conducted experiments and their results. The implementation code is available at <https://github.com/MikeZChi/GSPHAR.git>. Section 5 concludes the paper.

2 Background

This section reviews relevant concepts on graphs and GSP techniques. In addition, different baseline HAR models used in RV forecasting are reviewed.

2.1 Graph Theory Fundamentals

A graph can be denoted as $\mathcal{G} = (\mathcal{V}, \mathcal{E})$, where \mathcal{V} is the node set and \mathcal{E} is the edge set of the graph. An edge $e_{ij} \in \mathcal{E}$ can be formulated as $e_{ij} = (v_i, v_j)$, which indicates that the edge e_{ij} connects node v_i and node v_j . Edges can have attributes such as directions and weights. The direction of an edge defines how information flows between nodes, and the weight of an edge represents the importance or strength of the connection.

The adjacency matrix \mathbf{A} is used to capture the structure of graphs. If graph \mathcal{G} has N nodes, $\mathbf{A} \in \mathbb{R}^{N \times N}$. For an undirected graph, its adjacency matrix is always symmetric because if $(v_i, v_j) \in \mathcal{E}$, $(v_j, v_i) \in \mathcal{E}$ as well. Otherwise, the adjacency matrix of a directed graph is asymmetric. Elements in \mathbf{A} reflect the edge weights. Suppose the weight attached to edge e_{ij} is a positive real number w_{ij} . The formulation of the adjacency matrix is presented below:

$$\mathbf{A}_{ij} = \begin{cases} w_{ij}, & (v_i, v_j) \in \mathcal{E}; \\ 0, & (v_i, v_j) \notin \mathcal{E}. \end{cases} \quad (1)$$

The degree matrix D is formulated as $\mathbf{D} = \text{diag}(d_1, \dots, d_N)$, where $d_i = \sum_{j=1}^N \mathbf{A}_{ij}$.

2.2 GSP Based on the Magnetic Laplacian

A unified GSP framework can be applied to both undirected and directed graphs based on the magnetic Laplacian proposed by [Zhang et al. \(2021\)](#).

Suppose a directed graph \mathcal{G} has N nodes. In order to compute the magnetic Laplacian \mathbf{L}_m , the symmetric variant of adjacency matrix \mathbf{A}^s and the corresponding degree matrix \mathbf{D}^s should be firstly defined in Equation (2) and Equation (3), respectively,

$$\mathbf{A}^s = \frac{1}{2}(\mathbf{A} + \mathbf{A}^\top); \quad (2)$$

$$\mathbf{D}^s = \text{diag}\left(\sum_{j=1}^N \mathbf{A}_{1j}^s, \dots, \sum_{j=1}^N \mathbf{A}_{Nj}^s\right). \quad (3)$$

Besides, to capture the directional information, the phase matrix $\Theta^{(q)}$ is constructed as shown in Equation (4),

$$\Theta^{(q)} = 2\pi q(\mathbf{A} - \mathbf{A}^\top), \quad (4)$$

where q is a non-negative hyperparameter that determines how directional information is perceived and processed. Use i to represent the imaginary unit. Based on \mathbf{A}^s and $\Theta^{(q)}$, the complex Hermitian adjacency matrix $\mathbf{H}^{(q)}$ is defined in Equation (5),

$$\mathbf{H}^{(q)} = \mathbf{A}^s \odot \exp(i\Theta^{(q)}), \quad (5)$$

where \odot represents the element-wise multiplication between two matrices and $\exp(\cdot)$ is also the element-wise exponential transformation applied to each element of the input matrix.

A complex Hermitian matrix \mathbf{H} is a square matrix such that it is equal to its conjugate transpose: $\mathbf{H} = \mathbf{H}^\dagger$, which means $\mathbf{H}_{ij} = \overline{\mathbf{H}_{ji}}$ and $\overline{\mathbf{H}_{ji}}$ is the complex conjugate of element \mathbf{H}_{ij} . Furthermore, the unnormalized and normalized magnetic Laplacians can be formulated in Equations (6) and (7), respectively,

$$\mathbf{L}_m^{(q)} = \mathbf{D}^s - \mathbf{H}^{(q)}; \quad (6)$$

$$\widetilde{\mathbf{L}}_m^{(q)} = \mathbf{I} - ((\mathbf{D}^s)^{-\frac{1}{2}} \mathbf{A}^s (\mathbf{D}^s)^{-\frac{1}{2}}) \odot \exp(i\Theta^{(q)}). \quad (7)$$

Different q values represent different handlings of the directionality of the graph. For example, if $q = 0$, $\mathbf{H}^{(0)} = \mathbf{A}^s$. The directionality of the graph is eliminated through symmetrizing the asymmetric adjacency matrix. Thus, if the graph \mathcal{G} is undirected, q is fixed to 0. If $q = 0.25$, $\mathbf{L}_m^{(0.25)} = -(\mathbf{L}_m^{(0.25)})^\top$ when there is only one directed edge between any two connected nodes of \mathcal{G} .

Take the normalized magnetic Laplacian matrix $\widetilde{\mathbf{L}}_m^{(q)}$ as an example. Its eigendecomposition can be formulated in Equation (8) below:

$$\widetilde{\mathbf{L}}_m^{(q)} = \mathbf{U}_m \Lambda_m \mathbf{U}_m^\dagger, \quad (8)$$

where columns in \mathbf{U}_m are the orthonormal basis of eigenvectors of $\widetilde{\mathbf{L}}_m^{(q)}$ and \mathbf{U}_m^\dagger is the conjugate transpose of \mathbf{U}_m . It has been proved that \mathbf{U}_m and \mathbf{U}_m^\dagger are complex valued while eigenvalues in Λ_m are all real non-negative numbers (Zhang et al., 2021). This allows easy extensions of classical signal processing techniques to graphs.

The Graph Fourier Transformation (GFT) and its inverse (IGFT) for graph signal $\mathbf{x} \in \mathbb{R}^N$ based on normalized magnetic Laplacian are formulated in Equations (9) and (10), respectively,

$$\widetilde{\mathbf{x}} = \mathbf{U}_m^\dagger \mathbf{x}, \quad (9)$$

$$\mathbf{x} = \mathbf{U}_m \widetilde{\mathbf{x}}. \quad (10)$$

By adjusting the value of q , the magnetic Laplacian can suit both the undirected and direct graph structures and can process the directional information in the graphs as needed. When $q > 0$, the eigenvalue decomposition of the magnetic Laplacian leverages the graph directional information by extending the graph Fourier bases to the complex domain, while the eigenvalues remain non-negative real numbers as meaningful graph signal frequency measurements.

2.3 HAR Model and Its Extensions on Volatility Spillovers

The HAR framework is designed to account for the fact that different market participants (such as high frequency traders, institutional investors, and long-term investors) operate on different time horizons. The HAR model incorporates pooled RV data from these various time scales, typically daily, weekly and monthly, to represent the volatility behaviors. This design helps to capture the heterogeneous nature of volatility patterns in financial markets. Since the original RV data usually shows leptokurtosis (fat tails) and skewness, the log-transformed and square root versions of the RV data are often utilized to improve the forecasting accuracy of the HAR models.

Suppose \mathbf{v}_t contains the square root RV value of each of N stock market indices on day t : $\mathbf{v}_t = [(\text{RV}_{1,t})^{1/2}, (\text{RV}_{2,t})^{1/2}, \dots, (\text{RV}_{N,t})^{1/2}]$ and $\mathbf{v}_{t-n:t-m}$ is the average-pooled data: $\mathbf{v}_{t-n:t-m} = \frac{1}{n-m} \sum_{j=t-n}^{t-m} \mathbf{v}_j$. $\hat{\mathbf{v}}_t$ denotes the forecast square root RV value on day t . The conventional HAR model is formulated as:

$$\hat{\mathbf{v}}_t = \boldsymbol{\alpha} + \boldsymbol{\beta}_d \mathbf{v}_{t-1} + \boldsymbol{\beta}_w \mathbf{v}_{t-5:t-1} + \boldsymbol{\beta}_m \mathbf{v}_{t-22:t-1}, \quad (11)$$

where coefficients $\boldsymbol{\beta}_d$, $\boldsymbol{\beta}_w$ and $\boldsymbol{\beta}_m$ are diagonal matrices and they measure how the past daily, weekly and monthly volatility patterns influence future RVs. The intercept term $\boldsymbol{\alpha}$ is also a diagonal matrix. The HAR model cannot capture the comovement or correlations of the volatility in different stock markets, which limits its ability to deliver more accurate forecasts.

The GNNHAR model adds a l -layer spatial GNN component to the HAR model as an additional input variable to capture the volatility spillover effect as the complex interactions between nodes through neighborhood information aggregation and transformation. The GNNHAR model precomputes the volatility relational network \mathcal{G} with an adjacency matrix \mathbf{A} and a degree matrix \mathbf{D} which remain fixed during the

training process. The model is formulated as:

$$\begin{aligned}
\mathbf{H}^{(0)} &= [\mathbf{v}_{t-1}, \mathbf{v}_{t-5:t-2}, \mathbf{v}_{t-22:t-6}], \\
\mathbf{H}^{(1)} &= \text{ReLU}(\mathbf{D}^{-\frac{1}{2}} \mathbf{A} \mathbf{D}^{-\frac{1}{2}} \mathbf{H}^{(0)} \mathbf{W}^{(0)}), \\
&\dots, \\
\mathbf{H}^{(L+1)} &= \text{ReLU}(\mathbf{D}^{-\frac{1}{2}} \mathbf{A} \mathbf{D}^{-\frac{1}{2}} \mathbf{H}^{(L)} \mathbf{W}^{(L)}), \\
\widehat{\mathbf{v}}_t &= \boldsymbol{\alpha} + \beta_d \mathbf{v}_{t-1} + \beta_w \mathbf{v}_{t-5:t-2} + \beta_m \mathbf{v}_{t-22:t-6} \\
&\quad + \gamma \mathbf{H}^{(L+1)} + \epsilon_t.
\end{aligned} \tag{12}$$

Here, $\{\mathbf{W}^{(l)}\}_{l=0}^L$ are the trainable graph information transformation parameters, representing the linear information transformation, and $\text{ReLU}(\cdot)$ function transforms the graph information nonlinearly. γ is also a trainable parameter to measure the overall influence of related stock market indices. The GNNHAR model uses spatial GNNs to capture the nonlinear relationships between stock market indices and generates more accurate RV forecasts compared to the HAR model (Zhang et al., 2025). In addition, the GNNHAR model applies the same set of weights $\{\mathbf{W}^{(l)}\}_{l=0}^L$ to different parts of the volatility network to model the volatility spillover effect. This design ensures the GNNHAR model is scalable to large number of time series.

There are some other HAR model extensions such as the VHAR and HAR-KS models. These two models extend the linear combination of the HAR model to include historical volatility patterns of all entities in the system to generate RV forecasts for each target entity. However, they are less powerful than the GNNHAR model because: (a). they are less informative about the structure of the volatility network, and (b). they oversimplify the volatility spillover effect by assuming it is linear. Moreover, these models have potential scalability issue, as the number of parameters in both the VHAR and HAR-KS models grows quadratically as the number of relevant stock market indices increases. For further details, readers can refer to Bubák et al. (2011) for the VHAR model and Liang et al. (2020) for the HAR-KS model.

3 Methodology and Implementation

The proposed GSPHAR framework is introduced in this section. There are two proposed models, the basic GSPHAR model and the dynamic-GSPHAR (d-GSPHAR) model, under the GSPHAR framework. The d-GSPHAR model uses a simple yet effective method to model the dynamic volatility interconnections.

3.1 Model Formulation

In this section, the proposed GSPHAR model is introduced. The general workflow of the GSPHAR model is described in Figure 1 below:

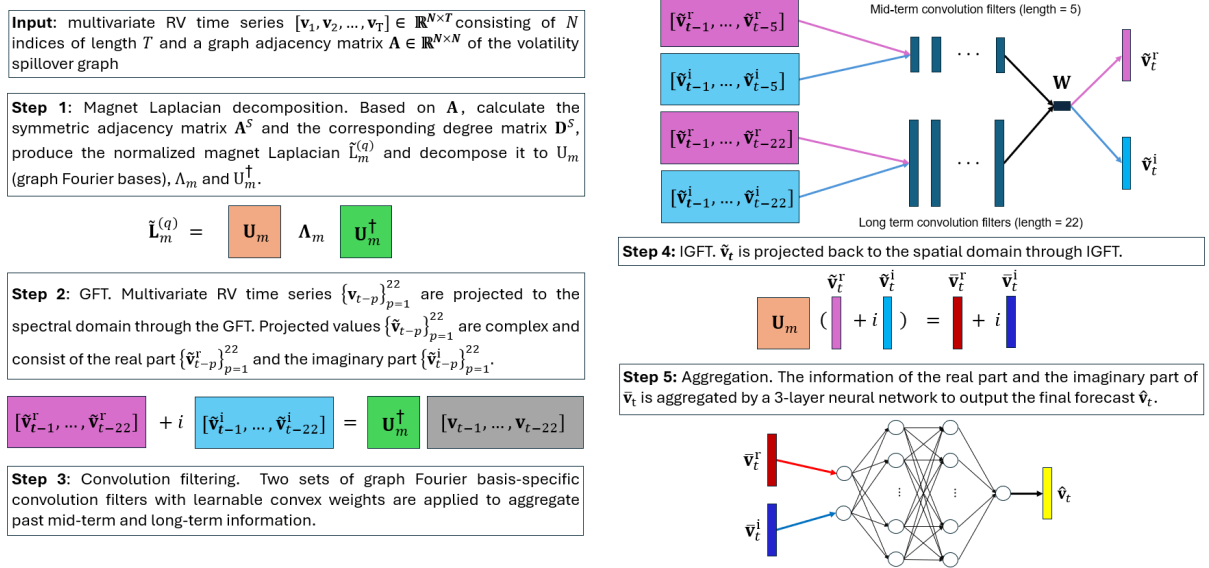


Figure 1: GSPHAR model architecture.

Now we present the detailed step-by-step development of the proposed framework. Suppose that the RV time series $\{\mathbf{v}_t \in \mathbb{R}^N\}_{t=1}^T$ consist of the RV time series of N different stock market indices from time $t = 1$ to time $t = T$. In the first step, the volatility spillover graph should be determined. Methods such as the Pearson correlation method and the Graphical LASSO (GLASSO) method (Friedman et al., 2007) only produce symmetric matrices to represent pairwise connections between stock markets. These methods do not capture the directional transmission of volatility. Influential stock markets tend to transmit more volatility to impressionable stock markets, whereas impressionable stock markets have minimal influence on influential stock markets. As a result, an alternative approach, the Diebold and Yilmaz (DY) framework (Diebold and Yilmaz, 2012), is applied to account for these asymmetric and directional effects. Specifically, the net pairwise volatility spillover effect matrix is calculated under the DY framework and is used as the adjacency matrix \mathbf{A}^{DY} of the volatility spillover graph. \mathbf{A}^{DY} can effectively highlight the dominant channels of volatility transmission, which allows researchers to pinpoint the markets that exert the most significant influence over others. The detailed calculation process of the net pairwise volatility spillover effect matrix can be found in Appendix B.

Based on the adjacency matrix \mathbf{A}^{DY} , the normalized magnet Laplacian matrix of the volatility spillover graph can be calculated based on the process described from Equation (2) to Equation (7) with $\mathbf{A} = \mathbf{A}^{DY}$. To learn from the directional volatility spillover effect, the hyperparameter q of the magnetic Laplacian

should be positive. Since there is only one directed edge exists between any two connected nodes in the net pairwise volatility spillover graph, $q = 0.25$ is chosen for better clarity and interpretability. Since $q = 0.25$, the eigendecomposition of the magnetic Laplacian $\tilde{\mathbf{L}}_m^{(0.25)}$ returns two eigenvector matrices, \mathbf{U}_m and \mathbf{U}_m^\dagger , in the complex space and one eigenvalue matrix, Λ_m , containing non-negative real numbers in its diagonal as shown in Equation (8). Thus, the RV time series input $[\mathbf{v}_{t-1}, \mathbf{v}_{t-2}, \dots, \mathbf{v}_{t-22}] \in \mathbb{R}^{N \times 22}$ can be projected to the spectral domain through the GFT:

$$[\tilde{\mathbf{v}}_{t-1}, \tilde{\mathbf{v}}_{t-2}, \dots, \tilde{\mathbf{v}}_{t-22}] = \mathbf{U}_m^\dagger [\mathbf{v}_{t-1}, \mathbf{v}_{t-2}, \dots, \mathbf{v}_{t-22}]. \quad (13)$$

Here, each projected value in $\{\tilde{\mathbf{v}}_{t-p}\}_{p=1}^{22}$ is complex valued and can be written as: $\tilde{\mathbf{v}}_{t-p} = \tilde{\mathbf{v}}_{t-p}^r + i\tilde{\mathbf{v}}_{t-p}^i$. The projected RV data merges the volatility information between different stock markets under the guidance of the volatility spillover graph. The GSPHAR model is designed to consistently process information from both the real and imaginary domains, following a similar approach as the HAR model.

The HAR family of models always applies an equal-weight average to construct the volatility pattern features based on the historical RV data. This assumption can be potentially improved. For example, under the simple design of the conventional HAR model in Equation (11), RV_{t-2} and RV_{t-5} always exert the same influence on the forecast RV_t . This equal weighting may not be able to sufficiently account for the dynamics of financial markets where the influence of past volatility on future volatility typically diminishes over time. This diminishing influence not only exists between short-term, mid-term and long-term, but also possibly occurs within different periods. To handle such potential insufficiency, a set of graph Fourier basis-specific convolution filters with learnable convex weights is applied to aggregate past information in the mid-term and long-term:

$$\begin{aligned} \tilde{\mathbf{v}}_{i,t-n:t-1} &= \sum_{j=t-n}^{t-1} w_{i,j} \tilde{\mathbf{v}}_{i,j}, \\ \text{s.t. } & \sum_{j=t-n}^{t-1} w_{i,j} = 1, w_{i,j} \geq 0 \end{aligned} \quad (14)$$

where $i \in 1, \dots, N$, each $w_{i,j}$ is a learnable non-negative weight in the convolution filter. The sum of all $w_{i,j}$ for each i is equal to 1 so that the weights are convex. In this way, the relative importance of each past RV observation can be easily depicted and compared with the weights in the original HAR model. The convolution filters are applied to the projected RV data so that it can aggregate (smooth) the spectral signals for each channel (time lag unit j) on each graph Fourier basis (each column in \mathbf{U}_m). Two distinct

sets of convolution filters are applied to the mid-term and long-term spectral RV data, whereas the same set of convolution filters is used for both the real and imaginary parts of the spectral RV data within each time period. To analyze the overall impact of each time lag unit j , weights in each set of filters are averaged across all N graph Fourier bases.

Hereafter, the HAR model is built for the real and imaginary parts of the spectral RV inputs, respectively. For clarity, let $\tilde{\mathbf{V}}_{t-22:t-1} = [\mathbf{1}, \tilde{\mathbf{v}}_{t-1}, \tilde{\mathbf{v}}_{t-5:t-1}, \tilde{\mathbf{v}}_{t-22:t-1}] \in \mathbb{R}^{N \times 4}$ to denote a collection of intercept terms and past short-term, mid-term and long-term spectral volatility patterns. The matrix $\mathbf{W} \in \mathbb{R}^{4 \times 1}$ contains the linear transformation parameters used in the HAR model. Here, superscript ‘r’ is used to denote the real component and superscript ‘i’ represents the imaginary component. The same set of HAR coefficients is applied to both real and imaginary parts to aggregate the historical spectral volatility pattern. The real and imaginary parts of the spectral RV forecast $\tilde{\mathbf{v}}_t$ are formulated as:

$$\begin{aligned}\tilde{\mathbf{v}}_t^r &= \tilde{\mathbf{V}}_{t-22:t-1}^r \mathbf{W}, \\ \tilde{\mathbf{v}}_t^i &= \tilde{\mathbf{V}}_{t-22:t-1}^i \mathbf{W}.\end{aligned}\tag{15}$$

Set $\tilde{\mathbf{v}}_t = \tilde{\mathbf{v}}_t^r + i\tilde{\mathbf{v}}_t^i$, which is still complex. $\tilde{\mathbf{v}}_t$ is projected back to the spatial domain through the IGFT:

$$\bar{\mathbf{v}}_t = \mathbf{U}_m \tilde{\mathbf{v}}_t.\tag{16}$$

The complex valued $\bar{\mathbf{v}}_t$ is divided into its real and imaginary parts again: $\bar{\mathbf{v}}_t = \bar{\mathbf{v}}_t^r + i\bar{\mathbf{v}}_t^i$. In the spatial domain, the information of the real part and the imaginary part of $\bar{\mathbf{v}}_t$ is aggregated by a 3 layer neural network $NN(\cdot)$ to output the final forecast: $\hat{\mathbf{v}}_t = NN(\bar{\mathbf{v}}_t^r, \bar{\mathbf{v}}_t^i)$. The shallow neural network can merge the volatility information in the real and imaginary domains in a nonlinear way, which effectively enhances the expressiveness of the proposed GSPHAR model. Furthermore, the growth rate of the parameters remains linear with respect to the number of stock market indices included. This ensures that the GSPHAR model is not only powerful, but also scalable to large volatility systems.

3.2 Dynamic Modeling

The pattern of the volatility spillover effect can vary across time because market conditions, economic factors and investor behavior continuously change, which reflects different periods of strengthened or weakened correlations (Diebold and Yilmaz, 2012; Antonakakis et al., 2018; Gong et al., 2021). However, there is a paucity of work on incorporating the dynamic volatility spillover effect into RV forecasting

models. The proposed GSPHAR model offers potential solutions to handle the changing correlations in the global stock market. It merges the volatility spillover effect into the RV data through GFT, in which the volatility network is precomputed and independent of the model training process. As long as the volatility network varies across different inputs, the model can become sensitive to the changes in volatility dynamics and adapt to the latest volatility patterns. However, how to change the volatility network with respect to the input RV data is an open question.

To address this, we propose a simple yet effective dynamic volatility spillover graph construction method based on both the DY framework and the Pearson correlation coefficient matrix of the input RV data. The DY framework is used to calculate the volatility network \mathbf{A}^{DY} based on the whole in-sample dataset. \mathbf{A}^{DY} can be interpreted as the average or overall volatility interconnection patterns during the in-sample period. The absolute Pearson correlation coefficient matrix $|\mathbf{A}^{\text{P}}|$ of the selected indices is calculated based on each RV input $\{\mathbf{v}_{t-p}\}_{p=1}^{22}$ of the HAR model. Specifically, two absolute Pearson correlation coefficient matrices, $|\mathbf{A}_{t-5:t-1}^{\text{P}}|$ and $|\mathbf{A}_{t-22:t-1}^{\text{P}}|$, are constructed based on the mid-term and long-term lagged RV input, respectively. For simplicity, the non-negative correlation coefficient matrices $|\mathbf{A}_{t-5:t-1}^{\text{P}}|$ and $|\mathbf{A}_{t-22:t-1}^{\text{P}}|$ are applied to the DY framework adjacency matrix \mathbf{A}^{DY} in a element-wise basis to produce the updated adjacency matrix \mathbf{A} :

$$\mathbf{A} = \rho |\mathbf{A}_{t-5:t-1}^{\text{P}}| \odot \mathbf{A}^{\text{DY}} + (1 - \rho) |\mathbf{A}_{t-22:t-1}^{\text{P}}| \odot \mathbf{A}^{\text{DY}}, \quad (17)$$

where ρ is a non-negative hyperparameter to balance the influence of mid-term historical RVs and long-term historical RVs when calculating \mathbf{A} . The outcome matrix \mathbf{A} is leveraged to calculate the magnetic Laplacian matrix, which is used in the GSPHAR model. The correlation coefficient matrices $|\mathbf{A}_{t-5:t-1}^{\text{P}}|$ and $|\mathbf{A}_{t-22:t-1}^{\text{P}}|$ can be regarded as a modification or adjustment applied to the magnitude of the overall volatility interconnection pattern \mathbf{A}^{DY} such that the overall volatility network is adjusted towards more recent RV data. A GSPHAR model that incorporates such dynamic designs is referred to as the dynamic-GSPHAR (d-GSPHAR) model.

4 Experiments

This section empirically evaluates the performance of the proposed GSPHAR and d-GSPHAR models, using square root RV time series from 24 stock market indices. The experiments are designed to compare these proposed models against baseline models to evaluate the validity and effectiveness of the GSPHAR

model and to uncover new empirical insights into RV dynamics. The usefulness of the convolution filters in the GSPHAR model is also investigated. Furthermore, the d-GSPHAR model is compared with the GSPHAR model to determine the effect of incorporating volatility dynamics into the proposed framework.

4.1 Model Evaluation Tools

Various evaluation criteria are applied to evaluate the effectiveness of the proposed models. The evaluation process is conducted on an index-wise basis, as different markets operate under different economic conditions and investor behaviors. Especially, the accuracy of out-of-sample RV forecasts is measured through the commonly used Mean Absolute Error (MAE, calculation detail to be shown in the following Section 4.3). In addition, the Model Confidence Set (MCS) test (Hansen et al., 2011) and the Diebold-Mariano (DM) test (Diebold and Mariano, 1995) are applied to compare the accuracy of out-of-sample forecasts between the proposed models and baseline models to assess whether the improvement is significant or not. Similar to the input settings of the HAR models, the out-of-sample forecasting windows are set as $H = 1, 5, 22$, corresponding to the short-term (daily), mid-term (weekly) and long-term (monthly) forecasting.

The software and hardware configurations are:

- Software: Python 3.10.14; NumPy 1.26.4; Statsmodels 0.14.2; PyTorch 1.13.1+cu116.
- Hardware: Operating system: Windows 11; CPU: 13th Gen Intel(R) Core(TM) i9-13900HX; GPU: NVIDIA GeForce RTX 4080 Laptop GPU.

4.2 Benchmark Datasets and Baseline models

The benchmark dataset consists of the square root RV data of 24 stock market indices with around 3500 common trading days from May 2002 to June 2022. Among them, some indices are commonly used indices in previous RV forecast research e.g., Liang et al. (2020). The daily RV data is produced based on the 5-minute intraday high frequency returns. Given that RV forecast models are trained on RV observations on common trading days of the included stock market indices, the selection of these 24 indices is intentionally focused on markets with more overlapping trading schedules. This approach ensures that the RV time series can be more continuous with more synchronized trading days across different markets, thus improving the data usage efficiency and enhancing the reliability and comparability of the RV forecasts produced by different models. The first 70% of data (from May 2002 to Feb 2016) are the in-sample data, whereas the

last 30% of data (from March 2016 to June 2022) are the out-sample data. Besides, the square root RV is scaled up by multiplying 100.

A descriptive analysis of the scaled square-rooted data for each stock market index is reported in Table 11 in Appendix A. The Augmented Dickey-Fuller (ADF) test (MacKinnon, 1994; Cheung and Lai, 1995) is conducted and results reject the existence of the unit root in each time series at the 5% significance level. This indicates that the time series data are stationary. As illustrated in the Volatility Spillover Graph Formulation section, the DY framework is applied to measure the net pairwise volatility spillover effect between different stock market indices. The net volatility spillover graph of the 24 stock market indices is presented below. The nodes represent different indices and the numbers on the edges measure the net pairwise volatility spillover effect. Larger values indicate stronger volatility spillover effects while smaller values reflect weaker volatility transmission.

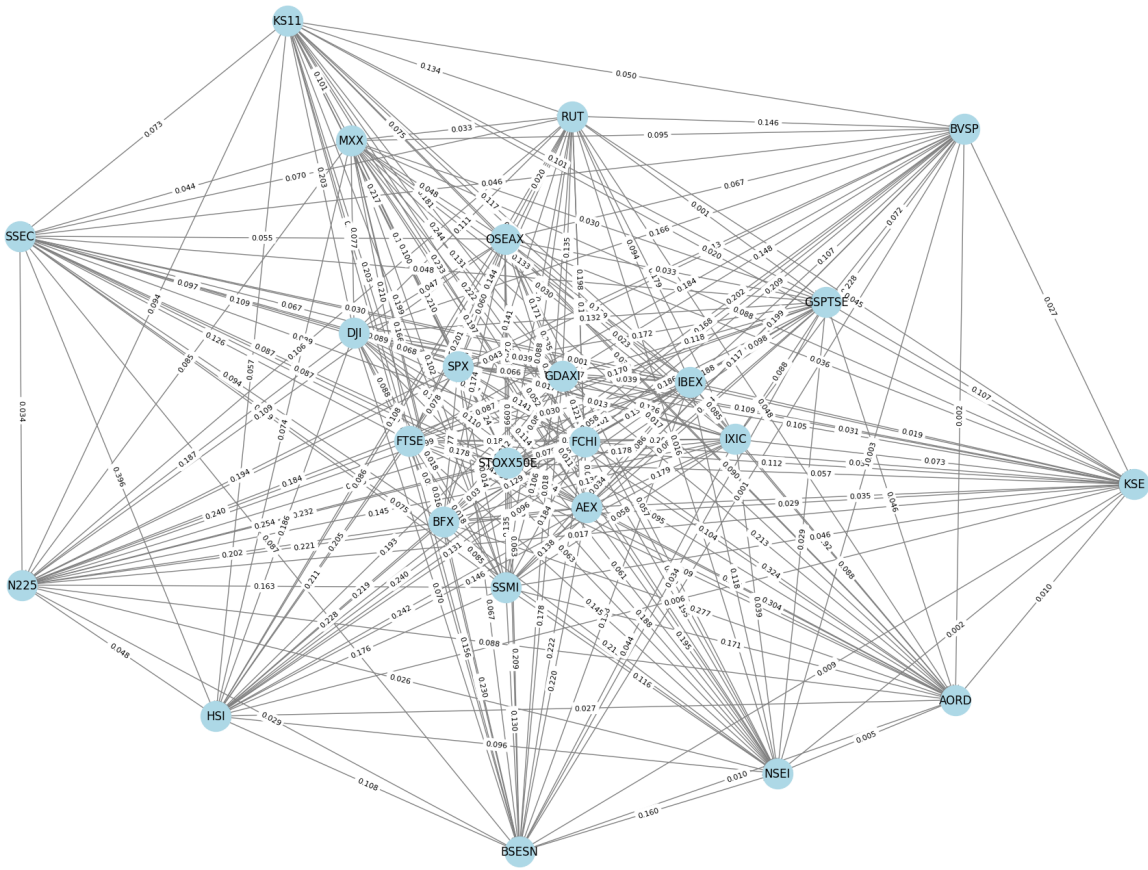


Figure 2: Net volatility spillover graph.

The baseline models include the HAR, VHAR, HAR-KS and GNNHAR models. Although the exact construction of some baseline models is not available, they are formulated according to the corresponding research papers. Notably, for the GNNHAR model, different values are tried for the hyperparameter L

and only the best performance is presented in each RV forecasting task. The relevant dataset and the code of the proposed models can be found at <https://github.com/MikeZChi/GSPHAR.git>.

4.3 Experiment Results

The general index-wise performance of each model is measured by the MAE calculated as follows:

$$\text{MAE}_i = \frac{1}{T_{\text{out}}} \sum_{t=1}^{T_{\text{out}}} |\hat{\mathbf{v}}_{i,t} - \mathbf{v}_{i,t}|, \quad (18)$$

where MAE_i is the MAE of the i_{th} stock market index and T_{out} denotes the duration of the out-of-sample dataset. $\hat{\mathbf{v}}_{i,t}$ refers to the square root RV forecasting value of the i_{th} index at time t and $\mathbf{v}_{i,t}$ is the true square root RV value of the i_{th} index at time t . The index-wise MAE results produced by each model with different forecasting horizon ($h = 1, 5, 22$) are presented in Tables 1, 2 and 3.

Table 1: MAE comparison of models across different stock market indices in the short-term forecasting task. Minimum MAE values for each index are highlighted in bold. The second smallest MAE values for each index are underlined.

$h = 1$	HAR	VHAR	HAR-KS	GNNHAR	GSPHAR
FCHI	0.191	0.224	0.200	<u>0.189</u>	0.186
AEX	0.182	0.201	0.189	<u>0.180</u>	0.174
BFX	0.177	0.182	<u>0.171</u>	0.173	0.168
STOXX50E	0.229	0.246	0.232	<u>0.228</u>	0.221
IBEX	0.203	0.247	0.224	<u>0.200</u>	0.194
GDAXI	<u>0.178</u>	0.214	0.195	0.178	0.168
AORD	0.177	0.175	<u>0.169</u>	0.175	0.168
FTSE	0.233	0.232	<u>0.229</u>	0.232	0.221
MXX	<u>0.170</u>	0.182	0.176	0.175	0.168
IXIC	0.213	0.222	0.215	<u>0.212</u>	0.209
SMMI	0.134	0.156	0.153	<u>0.130</u>	0.128
SPX	0.196	0.216	0.209	<u>0.192</u>	0.188
RUT	0.203	0.200	<u>0.198</u>	0.200	0.197
DJI	0.194	0.21	0.201	<u>0.186</u>	0.183
BSESN	0.176	0.202	0.191	<u>0.170</u>	0.159
NSEI	0.179	0.216	0.199	<u>0.172</u>	0.159
KS11	0.141	0.143	0.146	<u>0.139</u>	0.131
BVSP	0.211	0.249	0.218	<u>0.203</u>	0.197
HSI	0.155	0.169	0.160	<u>0.153</u>	0.147
KSE	0.200	0.203	0.206	<u>0.195</u>	0.187
N225	0.191	0.188	0.186	<u>0.185</u>	0.173
SSEC	0.178	0.209	0.192	<u>0.176</u>	0.163
OSEAX	0.269	0.267	<u>0.253</u>	0.268	0.248
GSPTSE	0.132	0.151	0.154	<u>0.125</u>	0.124

Table 2: MAE comparison of models across different stock market indices in the mid-term forecasting task. Minimum MAE values for each index are highlighted in bold. The second smallest MAE values for each index are underlined.

$h = 5$	HAR	VHAR	HAR-KS	GNNHAR	GSPHAR
FCHI	<u>0.253</u>	0.368	0.263	0.255	0.236
AEX	<u>0.242</u>	0.325	0.252	0.242	0.222
BFX	0.225	0.277	0.225	<u>0.223</u>	0.211
STOXX50E	0.295	0.404	0.310	<u>0.292</u>	0.272
IBEX	0.265	0.398	0.287	<u>0.263</u>	0.24
GDAXI	<u>0.237</u>	0.343	0.250	0.242	0.222
AORD	0.210	0.228	0.204	0.201	<u>0.204</u>
FTSE	0.279	0.320	0.274	<u>0.264</u>	0.261
MXX	<u>0.193</u>	0.235	0.194	0.219	0.190
IXIC	0.294	0.321	0.290	<u>0.285</u>	0.282
SSEMI	0.180	0.250	0.189	0.169	0.165
SPX	0.280	0.342	0.283	0.260	<u>0.265</u>
RUT	0.264	0.288	<u>0.261</u>	0.261	0.259
DJI	0.266	0.321	0.267	0.245	<u>0.250</u>
BSESN	0.236	0.313	0.263	<u>0.230</u>	0.199
NSEI	0.242	0.342	0.277	<u>0.236</u>	0.197
KS11	0.183	0.185	0.184	<u>0.182</u>	0.167
BVSP	0.274	0.369	0.273	0.246	<u>0.253</u>
HSI	<u>0.186</u>	0.217	0.189	0.191	0.177
KSE	0.237	0.239	<u>0.231</u>	0.240	0.220
N225	0.250	0.272	0.250	<u>0.224</u>	0.223
SSEC	0.240	0.309	0.271	<u>0.222</u>	0.199
OSEAX	0.317	0.402	0.317	<u>0.297</u>	0.289
GSPTSE	0.181	0.231	0.196	<u>0.175</u>	0.167

Table 3: MAE comparison of models across different stock market indices in the long-term forecasting task. Minimum MAE values for each index are highlighted in bold. The second smallest MAE values for each index are underlined.

$h = 22$	HAR	VHAR	HAR-KS	GNNHAR	GSPHAR
FCHI	0.302	0.451	0.341	<u>0.287</u>	0.271
AEX	0.290	0.366	0.306	<u>0.278</u>	0.262
BFX	<u>0.256</u>	0.306	0.265	0.263	0.242
STOXX50E	0.351	0.477	0.388	<u>0.336</u>	0.308
IBEX	0.303	0.484	0.360	<u>0.303</u>	0.270
GDAXI	0.287	0.402	0.322	<u>0.264</u>	0.248
AORD	0.248	0.259	0.249	<u>0.247</u>	0.236
FTSE	0.329	0.366	0.338	<u>0.327</u>	0.303
MXX	<u>0.214</u>	0.270	0.218	0.269	0.211
IXIC	<u>0.353</u>	0.390	0.358	0.368	0.337
SSEMI	0.237	0.297	0.243	0.209	<u>0.210</u>
SPX	0.354	0.433	0.379	<u>0.333</u>	0.319
RUT	<u>0.310</u>	0.355	0.319	0.335	0.300
DJI	0.341	0.398	0.365	<u>0.321</u>	0.305
BSESN	0.307	0.406	0.319	<u>0.246</u>	0.239
NSEI	0.315	0.422	0.328	<u>0.248</u>	0.242
KS11	0.221	0.256	0.217	<u>0.212</u>	0.195
BVSP	0.351	0.486	0.367	<u>0.343</u>	0.319
HSI	<u>0.214</u>	0.272	0.233	0.222	0.204
KSE	0.281	0.358	0.267	<u>0.264</u>	0.255
N225	0.299	0.303	0.310	<u>0.259</u>	0.248
SSEC	0.313	0.424	0.362	0.240	<u>0.243</u>
OSEAX	0.376	0.492	0.393	<u>0.368</u>	0.336
GSPTSE	0.234	0.323	0.276	0.205	<u>0.206</u>

According to the MAE results in Tables 1, 2 and 3, it is clear that the GSPHAR model improves RV forecasting results over all three forecast horizons. The GSPHAR model achieves the minimum MAE scores for 24, 20 and 21 stock market indices in the short-term ($h = 1$), mid-term ($h = 5$) and long-term ($h = 22$) RV forecasting tasks, respectively. Even when it does not achieve the best performance, the

GSPHAR model still produces the second smallest MAE scores. These imply the consistent superiority of the GSPHAR model in different forecasting horizons. Besides, linear HAR models are inferior to the GSPHAR model and the GNNHAR model. This implies that the linearity is insufficient in capturing the complex volatility spillover patterns.

Although the MAE score tables have shown the improved performance of the GSPHAR model, further backtests are carried out to validate whether these improvements are statistically significant. At a specified significance level, the MCS test evaluates all tested models to determine a subset of models that has statistically superior forecasting accuracy (based on MAE) for each market index. On the 5% significance level, the results of the MCS test for the models under different forecasting horizons are presented in Tables 4, 5, and 6.

Table 4: The MCS test results table of the short-term forecasting task with bold numbers representing that the corresponding models are included in the MCS at the 5% significance level.

$h = 1$	HAR	VHAR	HAR-KS	GNNHAR	GSPHAR
FCHI	0.107	0	0.044	0.182	1
AEX	0.001	0	0	0.001	1
BFX	0.002	0.002	0.336	0.015	1
STOXX50E	0.059	0.003	0.059	0.059	1
IBEX	0.003	0	0	0.034	1
GDAXI	0.001	0	0	0.001	1
AORD	0.024	0.059	0.781	0.035	1
FTSE	0.003	0.133	0.168	0.005	1
MXX	0.265	0.001	0.128	0.007	1
IXIC	0.064	0	0.014	0.074	1
SSMI	0.005	0	0	0.237	1
SPX	0.003	0	0	0.121	1
RUT	0.019	0.615	0.948	0.479	1
DJI	0	0	0	0.115	1
BSESN	0	0	0	0	1
NSEI	0	0	0	0	1
KS11	0	0	0	0.005	1
BVSP	0	0	0	0.042	1
HSI	0.009	0.001	0.009	0.009	1
KSE	0	0	0	0.002	1
N225	0	0	0	0	1
SSEC	0	0	0	0	1
OSEAX	0	0	0.380	0	1
GSPTSE	0	0	0	0.731	1

Table 5: The MCS test results table of the mid-term forecasting task with bold numbers representing that the corresponding models are included in the MCS at the 5% significance level.

$h = 5$	HAR	VHAR	HAR-KS	GNNHAR	GSPHAR
FCHI	0	0	0	0	1
AEX	0.004	0	0	0.002	1
BFX	0.011	0	0.011	0.011	1
STOXX50E	0	0	0	0.001	1
IBEX	0	0	0	0	1
GDAXI	0	0	0	0	1
AORD	0.086	0.001	0.753	1	0.753
FTSE	0.004	0	0.047	0.442	1
MXX	0.454	0	0.454	0	1
IXIC	0.033	0	0.075	0.403	1
SSMI	0.009	0	0	0.087	1
SPX	0.002	0	0	1	0.379
RUT	0.375	0.007	0.778	0.778	1
DJI	0.005	0	0.005	1	0.480
BSESN	0	0	0	0	1
NSEI	0	0	0	0	1
KS11	0.003	0.003	0.003	0.003	1
BVSP	0	0	0.002	1	0.161
HSI	0.021	0	0.021	0.007	1
KSE	0.001	0.006	0.009	0	1
N225	0	0	0.001	0.807	1
SSEC	0	0	0	0	1
OSEAX	0	0	0	0.012	1
GSPTSE	0.020	0	0	0.166	1

Table 6: The MCS test results table of the long-term forecasting task with bold numbers representing that the corresponding models are included in the MCS at the 5% significance level.

$h = 22$	HAR	VHAR	HAR-KS	GNNHAR	GSPHAR
FCHI	0.009	0	0	0.051	1
AEX	0.004	0	0.001	0.021	1
BFX	0.017	0	0.006	0.017	1
STOXX50E	0.001	0	0	0.007	1
IBEX	0.007	0	0	0.007	1
GDAXI	0	0	0	0.008	1
AORD	0.052	0.052	0.052	0.052	1
FTSE	0.007	0.001	0.004	0.007	1
MXX	0.594	0	0.509	0	1
IXIC	0.039	0.018	0.039	0.039	1
SSMI	0.001	0	0	1	0.887
SPX	0.014	0	0.001	0.200	1
RUT	0.087	0.006	0.032	0.012	1
DJI	0.006	0	0.001	0.128	1
BSESN	0	0	0	0.389	1
NSEI	0	0	0	0.390	1
KS11	0.004	0	0.008	0.021	1
BVSP	0.071	0	0.041	0.071	1
HSI	0.134	0	0.003	0.037	1
KSE	0.027	0	0.201	0.218	1
N225	0	0.005	0	0.175	1
SSEC	0	0	0	1	0.570
OSEAX	0.005	0	0	0.011	1
GSPTSE	0.003	0	0	1	0.920

According to the MCS test results, the GSPHAR model consistently remains in the MCS for all stock market indices in all short-term, mid-term and long-term forecasting tasks. On the other hand, other models stay in the MCS much less frequently.

The MAE results and the MCS test demonstrate that the GSPHAR model improved the RV forecasting performance compared to the other tested models. To further evaluate the RV forecasting results of the GSPHAR model across different forecasting horizons, the one-sided DM test is applied to perform pairwise comparisons against the competing models. Suppose the two candidate models are model 0 and model 1. The null hypothesis of the one-sided DM test is that model 0 and model 1 are indifferent or model 1 is inferior to model 0 in terms of forecast accuracy. When the DM test statistic is sufficiently large, the DM test can reject the null hypothesis and conclude that model 1 provides a significantly more accurate forecast than model 0. The results of the DM test are presented in Tables 7, 8 and 9. Here, for each DM test model 1 represents the GSPHAR model, and model 0 represents other models.

Table 7: The DM test results table of the short-term forecasting task with bold numbers represents that the GSPHAR is significantly better than the competing model at the 5% significance level.

$h = 1$	HAR vs GSPHAR		VHAR vs GSPHAR		HAR-KS-RV vs GSPHAR		GNNHAR vs GSPHAR	
	Index	DM Stats	p-Value	DM Stats	p-Value	DM Stats	p-Value	DM Stats
FCHI	2.414	0.008	9.383	0	3.332	0	1.808	0.035
AEX	7.361	0	27.021	0	14.82	0	5.877	0
BFX	9.260	0	14.242	0	3.035	0.001	5.439	0
STOXX50E	8.186	0	12.208	0	2.777	0.003	6.839	0
IBEX	8.216	0	15.957	0	6.455	0	4.776	0
GDAXI	10.085	0	37.947	0	6.074	0	6.184	0
AORD	4.613	0	3.610	0	0.770	0.221	3.804	0
FTSE	11.468	0	2.789	0.003	2.898	0.002	11.007	0
MXX	2.034	0.021	6.491	0	2.58	0.005	6.161	0
IXIC	3.711	0	6.044	0	6.441	0	3.112	0.001
SSMI	5.491	0	27.432	0	14.34	0	2.042	0.021
SPX	6.003	0	9.312	0	7.732	0	2.264	0.012
RUT	5.559	0	0.779	0.218	0.083	0.467	2.260	0.012
DJI	8.924	0	7.925	0	12.742	0	2.515	0.006
BSESN	17.734	0	9.389	0	9.085	0	11.219	0
NSEI	19.561	0	11.122	0	12.249	0	13.094	0
KS11	7.128	0	12.125	0	7.097	0	4.611	0
BVSP	10.374	0	8.513	0	10.490	0	4.150	0
HSI	5.070	0	13.739	0	2.889	0.002	3.393	0
KSE	12.620	0	6.263	0	10.527	0	4.666	0
N225	17.899	0	3.805	0	8.245	0	10.018	0
SSEC	14.961	0	6.670	0	14.393	0	12.338	0
OSEAX	20.460	0	18.208	0	4.175	0	19.028	0
GSPTSE	3.644	0	27.000	0	7.414	0	0.506	0.306

Table 8: The DM test results table of the mid-term forecasting task with bold numbers represents that the GSPHAR is significantly better than the competing model at the 5% significance level.

h = 5	HAR vs GSPHAR		VHAR vs GSPHAR		HAR-KS-RV vs GSPHAR		GNNHAR vs GSPHAR	
	Index	DM Stats	p-Value	DM Stats	p-Value	DM Stats	p-Value	DM Stats
FCHI	3.776	0	9.002	0	4.033	0	4.899	0
AEX	2.858	0.002	7.192	0	4.365	0	5.265	0
BFX	2.549	0.005	6.445	0	2.885	0.002	4.520	0
STOXX50E	3.957	0	9.735	0	5.205	0	6.182	0
IBEX	4.437	0	11.208	0	7.212	0	7.853	0
GDAXI	3.631	0	9.271	0	4.579	0	5.293	0
AORD	2.188	0.014	3.778	0	0.522	0.301	-1.418	0.922
FTSE	3.611	0	7.421	0	3.059	0.001	2.612	0.005
MXX	1.381	0.084	5.841	0	1.248	0.106	29.416	0
IXIC	2.969	0.001	4.505	0	2.844	0.002	3.356	0
SSMI	2.607	0.005	7.065	0	4.448	0	2.171	0.015
SPX	3.897	0	5.530	0	3.805	0	-1.358	0.913
RUT	1.900	0.029	3.065	0.001	0.611	0.271	0.908	0.182
DJI	4.193	0	4.990	0	2.985	0.001	-0.753	0.774
BSESN	5.572	0	8.433	0	8.362	0	6.293	0
NSEI	6.111	0	9.776	0	9.058	0	6.872	0
KS11	4.403	0	2.834	0.002	4.536	0	5.460	0
BVSP	2.941	0.002	5.760	0	2.332	0.010	-1.801	0.964
HSI	2.520	0.006	4.747	0	2.139	0.016	5.156	0
KSE	5.841	0	2.885	0.002	5.342	0	7.625	0
N225	6.927	0	4.755	0	4.412	0	0.300	0.382
SSEC	5.813	0	5.702	0	7.178	0	5.985	0
OSEAX	6.456	0	7.916	0	4.659	0	7.765	0
GSPTSE	3.541	0	6.612	0	5.534	0	1.704	0.044

Table 9: The DM test results table of the long-term forecasting task with bold numbers represents that the GSPHAR is significantly better than the competing model at the 5% significance level.

h = 22	HAR vs GSPHAR		VHAR vs GSPHAR		HAR-KS-RV vs GSPHAR		GNNHAR vs GSPHAR	
	Index	DM Stats	p-Value	DM Stats	p-Value	DM Stats	p-Value	DM Stats
FCHI	3.056	0.001	6.550	0	4.696	0	2.066	0.019
AEX	3.243	0.001	4.406	0	4.004	0	2.302	0.011
BFX	2.278	0.011	3.548	0	2.855	0.002	2.890	0.002
STOXX50E	3.488	0	6.351	0	4.853	0	2.968	0.002
IBEX	2.729	0.003	7.057	0	5.014	0	3.364	0
GDAXI	3.603	0	5.551	0	4.983	0	2.795	0.003
AORD	2.529	0.006	2.119	0.017	2.913	0.002	2.724	0.003
FTSE	3.048	0.001	3.396	0	3.567	0	3.254	0.001
MXX	0.610	0.271	3.835	0	1.117	0.132	7.176	0
IXIC	2.009	0.022	2.575	0.005	2.313	0.010	2.496	0.006
SSMI	3.234	0.001	4.484	0	3.569	0	-0.149	0.559
SPX	3.327	0	3.965	0	3.998	0	1.370	0.085
RUT	1.667	0.048	3.054	0.001	2.246	0.012	2.920	0.002
DJI	3.438	0	3.570	0	4.055	0	1.586	0.056
BSESN	4.805	0	6.721	0	4.738	0	0.762	0.223
NSEI	4.770	0	6.809	0	4.808	0	0.865	0.193
KS11	3.348	0	3.532	0	2.876	0.002	2.347	0.009
BVSP	1.782	0.037	4.378	0	2.217	0.013	2.042	0.021
HSI	1.461	0.072	3.727	0	2.915	0.002	2.840	0.002
KSE	2.780	0.003	4.719	0	2.019	0.022	1.171	0.121
N225	4.172	0	3.109	0.001	4.467	0	1.416	0.078
SSEC	3.797	0	4.616	0	5.387	0	-0.571	0.716
OSEAX	3.656	0	4.902	0	3.825	0	2.520	0.006
GSPTSE	4.156	0	4.627	0	5.507	0	-0.084	0.533

According to the DM test results in Tables 7, 8 and 9, in all short-term, mid-term and long-term forecasting tasks, the GSPHAR model has significantly higher RV forecasting accuracy compared to all baseline models, including the HAR, VHAR, HAR-KS-RV and GNNHAR models, for the majority of, if not all, the stock market indices. The significant superiority of the GSPHAR model demonstrates that, compared to other HAR model extensions, the GSPHAR model better incorporates the directional and nonlinear volatility spillover effect into the HAR framework. It also proves the effectiveness of including the spectral domain analysis in the spatio-temporal forecasting framework. Overall, the GSPHAR model can easily scale up to larger volatility networks, and it better captures the volatility spillover effect at the same time.

The HAR models utilize a simple average to aggregate past RV values, which implies equal importance of the lagged terms within the mid-term and long-term periods. However, the learnable weights of the convolutional filters of the GSPHAR model reveal that the importance of past RV information decays more dynamically and smoothly instead of in a step-wise manner. According to Figure 3, compared to the HAR model weights, the convolution filters put more weight on the $t - 1$ RV data, the short-term volatility pattern. This implies that the auto-regression in the volatility process is more reactive to recent market conditions. From time lag 2 to time lag 5, the learned weights of the GSPHAR model decrease from about 0.38 to 0.1 while the weights of HAR models remain constant at 0.2. This suggests that the HAR model potentially underestimates the importance of the more recent lag 2 volatility pattern and overestimates the importance of the volatility pattern of the subsequent lags in the mid-term period. A similar pattern can be detected in the long-term, where the learned weights initially exceed, then fluctuate around, and finally fall below the constant HAR weights. Although the general pattern of the constant weights of the HAR models is reasonable in that they do put more emphasis on more recent volatility patterns, the stepwise decline between each time period and the stability within each time period overlook the nuanced contributions of different time lags. On the other hand, the learnable weights indicate a more sophisticated understanding of how the influence of past RV values fades with time in the volatility auto-regression process and provide a more flexible representation that better captures the temporal relationships inherent in the data.

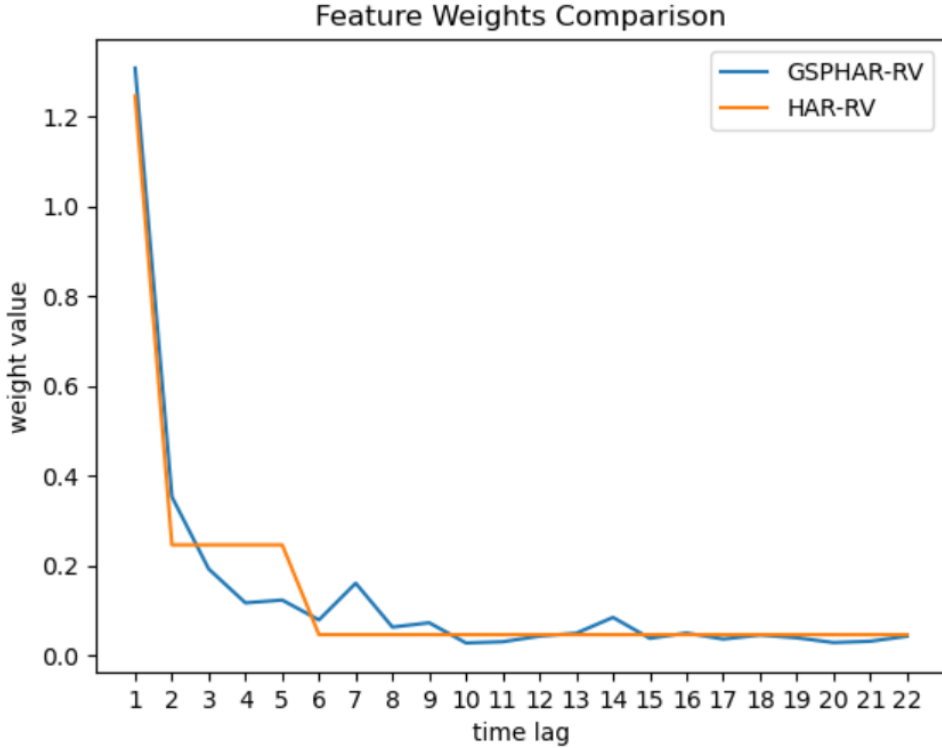


Figure 3: GSPHAR convolutional weights vs HAR model weights

Compared to the GNNHAR which uses a fixed optimizable hyperparameter l to capture the local volatility interdependencies, the GSPHAR model only relies on the precomputed adjacency matrix to capture the volatility spillover effect. This adjacency matrix can be updated easily as its construction is independent of the model training process. The d-GSPHAR is proposed to incorporate the changing volatility spillover networks by updating the adjacency matrix with correlation coefficient matrices, as described in Equation (17). To evaluate the benefits of the d-GSPHAR in RV forecasting, the index-wise MAE results produced by GSPHAR, the best model in previous comparisons, and d-GSPHAR with different forecasting horizons h are presented in Table 10. Although the MAE results between GSPHAR and d-GSPHAR are close in the short-term forecasting task, the d-GSPHAR improves the RV forecasting performances in the mid-term and long-term RV forecasting. These findings emphasizes the benefits of employing a dynamic graph structure to capture volatility spillover effects and improve the forecasting accuracy.

Table 10: MAE comparison between GSPHAR and d-GSPHAR across different stock market indices and different forecasting horizons. Smaller MAE values for each index and each forecasting horizon are highlighted in bold.

Index	Short-term ($h = 1$)		Mid-term ($h = 5$)		Long-term ($h = 22$)	
	GSPHAR	d-GSPHAR	GSPHAR	d-GSPHAR	GSPHAR	d-GSPHAR
FCHI	0.187	0.185	0.236	0.234	0.271	0.274
AEX	0.174	0.174	0.222	0.224	0.262	0.260
BFX	0.168	0.170	0.211	0.211	0.242	0.241
STOXX50E	0.221	0.217	0.272	0.269	0.308	0.308
IBEX	0.194	0.193	0.240	0.239	0.270	0.270
GDAXI	0.168	0.172	0.222	0.217	0.248	0.247
AORD	0.168	0.169	0.204	0.203	0.236	0.236
FTSE	0.221	0.221	0.261	0.260	0.303	0.301
MXX	0.168	0.167	0.19	0.189	0.211	0.208
IXIC	0.209	0.208	0.282	0.279	0.337	0.336
SSMI	0.128	0.126	0.165	0.164	0.210	0.211
SPX	0.188	0.191	0.265	0.260	0.319	0.318
RUT	0.197	0.197	0.259	0.254	0.300	0.299
DJI	0.183	0.184	0.25	0.245	0.305	0.304
BSESN	0.159	0.161	0.199	0.198	0.239	0.238
NSEI	0.159	0.162	0.197	0.198	0.242	0.241
KS11	0.131	0.134	0.167	0.165	0.195	0.196
BVSP	0.197	0.200	0.253	0.250	0.319	0.318
HSI	0.147	0.150	0.177	0.176	0.204	0.200
KSE	0.187	0.187	0.220	0.218	0.255	0.255
N225	0.173	0.177	0.223	0.220	0.248	0.247
SSEC	0.163	0.163	0.199	0.199	0.243	0.242
OSEAX	0.248	0.253	0.289	0.287	0.336	0.336
GSPTSE	0.124	0.124	0.167	0.164	0.206	0.206

5 Conclusion

This study examines the interconnections of global financial markets by analyzing volatility spillovers. It proposes a novel RV forecasting framework that combines the HAR model and GSP techniques based on the magnetic Laplacian. Results from the empirical tests on data from 24 global stock market indices show that, compared to baseline models, the GSPHAR model under the proposed GSPHAR framework significantly improves the RV forecasting accuracy. Unlike existing approaches where the volatility spillover effect is regarded as exogenous variables representing additional spatial information in the HAR framework to perform RV forecast, the proposed GSPHAR framework treats the volatility spillover effect as an integral component of the model’s design. The proposed framework uses GFT techniques to incorporate the volatility interrelationships into the HAR model inputs through spatial and spectral domain transformation. In addition, the directionality and nonlinearity of the volatility spillover effect are handled in the spatial domain with a shallow neural network. The superior experiment results indicate that the proposed GSPHAR framework is more effective than the HAR model and its extensions. Furthermore, the GSPHAR framework employs convolution filters with learnable parameters to reveal the more dynamic decaying pattern of the volatility auto-regression process. Besides, the d-GSPHAR model novelly integrates

the changing volatility spillover effect into the RV forecasting problem. The dynamic volatility network design allows the proposed model to capture the changing volatility interconnection pattern, which also enhances the forecasting accuracy.

An interesting future research direction can be how to efficiently and effectively design the dynamic volatility spillover graph. The dynamic graph structure should be timely adjusted in response to the evolving relationships among markets or changes in market behavior.

A RV Time Series Data Statistics

Table 11: Descriptive Statistics and ADF Test Results for the RV Dataset of Various Stock Market Indices

Index	Area	Mean	Std Dev	Skewness	Kurtosis	ADF Stats	ADF p-value
FCHI	France	0.959	0.541	2.349	9.241	-5.430	0
AEX	Netherlands	0.880	0.529	2.686	12.486	-7.681	0
BFX	Belgium	0.816	0.446	2.604	12.192	-4.782	0
STOXX50E	Eurozone	1.033	0.611	2.646	12.626	-6.699	0
IBEX	Spain	1.025	0.557	2.775	16.836	-5.268	0
GDAXI	Germany	1.001	0.598	2.461	9.298	-4.921	0
AORD	Australia	0.604	0.379	4.218	35.781	-6.052	0
FTSE	UK	0.884	0.548	3.479	25.224	-7.579	0
MXX	Mexico	0.758	0.409	3.547	29.078	-7.802	0
IXIC	USA	0.824	0.477	2.562	12.042	-8.098	0
SSMI	Switzerland	0.766	0.471	4.253	33.192	-6.750	0
SPX	USA	0.799	0.546	2.858	14.293	-8.293	0
RUT	USA	0.762	0.451	2.953	15.755	-8.718	0
DJI	USA	0.808	0.547	3.201	19.406	-8.508	0
BSESN	India	0.939	0.551	4.814	54.345	-8.831	0
NSEI	India	0.945	0.592	5.258	70.300	-8.937	0
KS11	South Korea	0.815	0.417	2.299	10.896	-4.590	0
BVSP	Brazil	1.063	0.495	2.834	15.739	-8.743	0
HSI	China (Hong Kong)	0.816	0.383	3.214	20.980	-4.657	0
KSE	Pakistan	0.832	0.513	2.542	10.339	-5.933	0
N225	Japan	0.824	0.432	3.053	20.018	-9.530	0
SSEC	China	1.085	0.682	2.445	9.384	-4.352	0
OSEAX	Norway	0.945	0.588	5.532	82.454	-9.911	0
GSPTSE	Canada	0.669	0.459	3.518	21.735	-5.183	0

B Volatility Spillover Effect Matrix Formulation Under DY Framework

Suppose a covariance stationary multi-asset volatility time series $\{\mathbf{v}_t \in \mathbb{R}^N\}_{t=1}^T$ consists of N assets. A p -order vector autoregressive model (VAR(p)) for these time series can be represented as:

$$\mathbf{v}_t = \sum_{i=1}^p \phi_i \mathbf{v}_{t-i} + \boldsymbol{\epsilon}_t, \quad \boldsymbol{\epsilon}_t \sim (0, \boldsymbol{\Sigma}_\epsilon), \quad (19)$$

where each ϕ_i is a scalar coefficient. This model can be rewritten in a moving average (MA) form:

$$\mathbf{v}_t = \sum_{i=1}^{\infty} \mathbf{B}_i \boldsymbol{\epsilon}_{t-i}, \quad (20)$$

where \mathbf{B}_i defined recursively by $\mathbf{B}_i = \sum_{j=1}^p \phi_j \mathbf{B}_{i-j}$ with the assumption that $\mathbf{B}_0 = \mathbf{I}_{N \times N}$ and $\mathbf{B}_i = 0$ for $i < 0$. By performing a variance decomposition of the H -step-ahead forecast error, each element in the

resulting matrix $\boldsymbol{\theta}^g(H)$ given by:

$$\boldsymbol{\theta}_{ij}^g(H) = \frac{\sigma_{jj}^{-1} \sum_{h=0}^{H-1} (\mathbf{e}_i^\top \mathbf{B}_h \boldsymbol{\Sigma}_\epsilon \mathbf{e}_j)^2}{\sum_{h=0}^{H-1} (\mathbf{e}_i^\top \mathbf{B}_h \boldsymbol{\Sigma}_\epsilon \mathbf{B}_h^\top \mathbf{e}_i)}, \quad (21)$$

where H is the forecast horizon and \mathbf{e}_i is a selection vector of dimension N with 1 in the i -th position and zeros elsewhere. To standardize this matrix such that each row sums to 1, the elements in the normalized matrix $\tilde{\boldsymbol{\theta}}^g(H)$ can be defined as:

$$\tilde{\boldsymbol{\theta}}_{ij}^g(H) = \frac{\boldsymbol{\theta}_{ij}^g(H)}{\sum_{j=1}^N \boldsymbol{\theta}_{ij}^g(H)}. \quad (22)$$

Furthermore, the net pairwise volatility spillovers $\bar{\boldsymbol{\theta}}^g(H)$ can be further calculated based on $\tilde{\boldsymbol{\theta}}^g(H)$:

$$\bar{\boldsymbol{\theta}}_{ij}^g(H) = \begin{cases} \tilde{\boldsymbol{\theta}}_{ij}^g(H) - \tilde{\boldsymbol{\theta}}_{ji}^g(H), & \tilde{\boldsymbol{\theta}}_{ij}^g(H) \geq \tilde{\boldsymbol{\theta}}_{ji}^g(H); \\ 0, & \tilde{\boldsymbol{\theta}}_{ij}^g(H) < \tilde{\boldsymbol{\theta}}_{ji}^g(H). \end{cases} \quad (23)$$

References

Andersen, T. G. and T. Bollerslev (1998). Answering the skeptics: Yes, standard volatility models do provide accurate forecasts. *International Economic Review* 39(4), 885–905.

Antonakakis, N., D. Gabauer, R. Gupta, and V. Plakandaras (2018). Dynamic connectedness of uncertainty across developed economies: A time-varying approach. *Economics Letters* 166, 63–75.

Bollerslev, T., B. Hood, J. Huss, and L. H. Pedersen (2018). Risk Everywhere: Modeling and Managing Volatility. *The Review of Financial Studies* 31(7), 2729–2773.

Bubák, V., E. Kočenda, and F. Žikeš (2011). Volatility transmission in emerging european foreign exchange markets. *Journal of Banking & Finance* 35(11), 2829–2841.

Cheung, Y.-W. and K. S. Lai (1995). Lag order and critical values of the augmented dickey–fuller test. *Journal of Business & Economic Statistics* 13(3), 277–280.

Corsi, F. (2009). A Simple Approximate Long-Memory Model of Realized Volatility. *Journal of Financial Econometrics* 7(2), 174–196.

Diebold, F. X. and R. S. Mariano (1995). Comparing predictive accuracy. *Journal of Business & Economic Statistics* 13(3), 253–263.

Diebold, F. X. and K. Yilmaz (2009). Measuring Financial Asset Return and Volatility Spillovers, with Application to Global Equity Markets. *The Economic Journal* 119(534), 158–171.

Diebold, F. X. and K. Yilmaz (2012). Better to give than to receive: Predictive directional measurement of volatility spillovers. *International Journal of Forecasting* 28(1), 57–66. Special Section 1: The Predictability of Financial Markets Special Section 2: Credit Risk Modelling and Forecasting.

Forbes, K. J. and R. Rigobon (2002). No contagion, only interdependence: Measuring stock market comovements. *The Journal of Finance* 57(5), 2223–2261.

Friedman, J., T. Hastie, and R. Tibshirani (2007). Sparse inverse covariance estimation with the graphical lasso. *Biostatistics* 9(3), 432–441.

Gong, X., Y. Liu, and X. Wang (2021). Dynamic volatility spillovers across oil and natural gas futures markets based on a time-varying spillover method. *International Review of Financial Analysis* 76, 101790.

Hansen, P. R., A. Lunde, and J. M. Nason (2011). The model confidence set. *Econometrica* 79(2), 453–497.

Kanas, A. (2000). Volatility spillovers between stock returns and exchange rate changes: International evidence. *Journal of Business Finance & Accounting* 27(3-4), 447–467.

Liang, C., Y. Wei, and Y. Zhang (2020). Is implied volatility more informative for forecasting realized volatility: An international perspective. *Journal of Forecasting* 39(8), 1253–1276.

MacKinnon, J. G. (1994). Approximate asymptotic distribution functions for unit-root and cointegration tests. *Journal of Business & Economic Statistics* 12(2), 167–176.

Patton, A. J. and K. Sheppard (2015). Good volatility, bad volatility: Signed jumps and the persistence of volatility. *Review of Economics and Statistics* 97(3), 683–697.

Poon, S.-H. and C. W. Granger (2003). Forecasting volatility in financial markets: A review. *Journal of Economic Literature* 41(2), 478–539.

Yang, Z. and Y. Zhou (2017). Quantitative easing and volatility spillovers across countries and asset classes. *Management Science* 63(2), 333–354.

Zhang, C., X. Pu, M. Cucuringu, and X. Dong (2025). Forecasting realized volatility with spillover effects: Perspectives from graph neural networks. *International Journal of Forecasting* 41(1), 377–397.

Zhang, X., Y. He, N. Brugnone, M. Perlmutter, and M. Hirn (2021). Magnet: A neural network for directed graphs. *Advances in Neural Information Processing Systems* 34, 27003–27015.